Dependence of Cooled Reverse-Flow Reactor Dynamics on Reactor Model

J. Khinast, Y. O. Jeong, and D. Luss
Dept. of Chemical Engineering, University of Houston, Houston, TX 77204

Extensive simulations indicate that in most but not all cases the single- and two-phase models predict similar dynamic behavior of a reverse-flow reactor, when catalyst pellet multiplicity does not occur at any point in the reactor. Differences in the predictions are found in some cases close to the dynamic bifurcation loci of a cooled RFR, or in others when the qualitative dynamic behavior is very sensitive to the value of the parameters, such as close to a transition to chaotic behavior. The two models can lead to rather different predictions of the dynamic features when there are large differences between the feed and coolant temperatures.

Introduction

A reverse-flow reactor (RFR) is a catalytic packed-bed reactor in which the flow direction of the reactants is periodically reversed to trap a hot zone within the reactor. Upon entering the reactor, the cold feed is heated up regeneratively by the hot bed as the high-temperature (reaction) front moves in the downstream direction. Before the hot reaction zone exits the reactor, the feed flow direction is reversed. The reactor is shown in Figure 1. The *flow-reversal period* t_f is usually constant and predefined and one complete RFR-cycle consists of two flow-reversal periods. Quasi-stationary behavior is reached after repeated flow reversals.

The RFR concept was first proposed and patented by Cottrell (1938) for the removal of pollutants. Frank-Kamenetskii (1955) described the oxidation of isopropyl-alcohol to acetone over a copper catalyst in an RFR. A patent for reduction of SO_2 in an RFR was issued to Watson (1975). Recent applications and studies of RFRs have been motivated by its successful application to SO_2 oxidation in Russia (Boreskov et al., 1979; Boreskov and Matros, 1983; Matros, 1989). Experimental investigations include the removal of NO_x (Bobrova et al., 1988), syngas-production (Blanks et al., 1990), methanol synthesis (Neophytides and Froment, 1992), the catalytic destruction of VOCs (Nieken et al., 1994; van de Beld, 1995), and catalytic oxidation of CO (Züfle and Turek, 1997). An extensive review of the applications and studies of the RFR was presented by Matros and Bunimovich (1996).

The input to the RFR changes periodically and an adiabatic operation leads to periodic, symmetric states at which the temperature (and concentration) profiles at the beginning and end of a flow-reversal period are mirror images. We call these states *symmetric period-1* operation. Laboratory and pilot-plant RFRs usually cannot be operated in an adiabatic mode (Matros, 1989; Züfle and Turek, 1997). Moreover, in some applications involving equilibrium-limited reactions cooling is applied to avoid exceeding some critical temperatures at which either undesired reactions or catalyst deactivation may occur. Various modes of RFR cooling were described by Matros and Bunimovich (1996). Reactor cooling

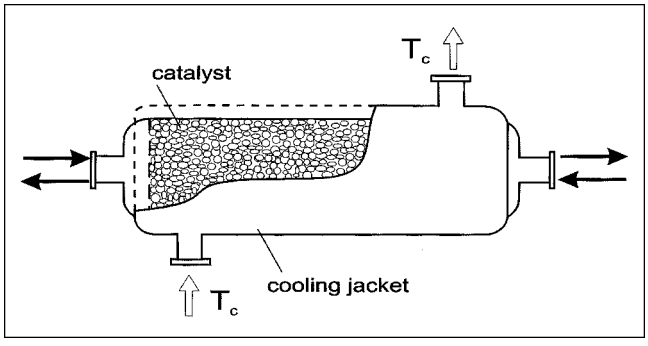

Figure 1. Cooled reverse-flow reactor.

Correspondence concerning this article should be addressed to D. Luss.
Current address of J. Khinast: Dept. of Chemical and Biochemical Engineering, Rutgers University, Piscataway, NJ 08854.
Current address of Y. O. Jeong: Dept. of Chemical Engineering, Pukyong National University, Yong-Dang-Dong, Nam-Ku, Pusan, South Korea.

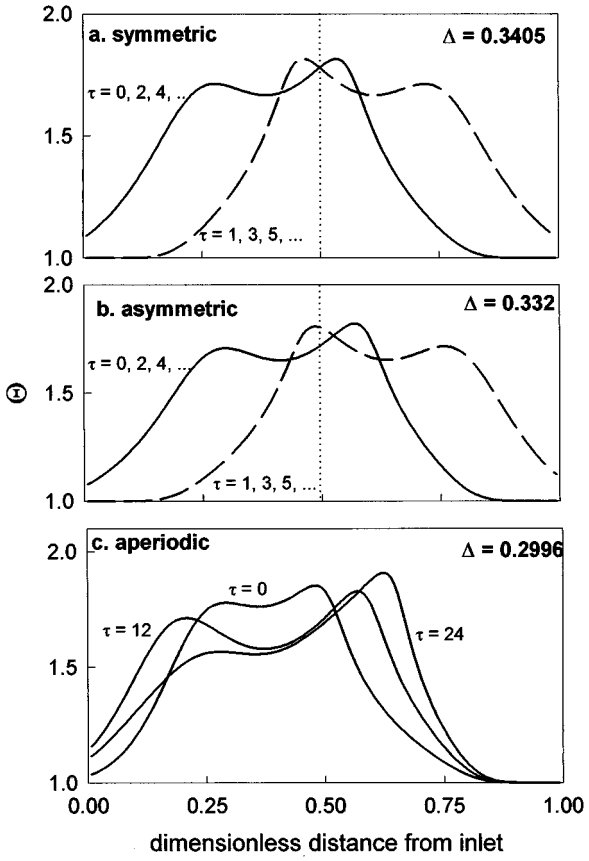

Figure 2. Dimensionless temperature profiles of an RFR before the flow direction switch for t_f=1,200 s.

$\tau = 1$ is the dimensionless flow-reversal period. (a) Symmetric period-1 state; (b) asymmetric period-1 state; (c) aperiodic state.

may introduce some complex and rich dynamic features, which do not exist in its absence (Rehacek et al., 1992, 1998; Salinger and Eigenberger, 1996b; Khinast et al., 1998). For example, under relatively fast flow-reversal frequencies the symmetric states of a cooled RFR may become unstable and either *asymmetric* or *aperiodic* states may be obtained. Aperiodic states may be either *quasi-periodic*, that is, in addition to the flow-reversal period (forcing frequency) a second period determines the over-all behavior, or *chaotic*. Examples of the dimensionless temperature profiles, that is, T/T_0, for these three types of states are shown in Figure 2, where $\tau = 1$ corresponds to one flow-reversal period. The differences in the dynamic features are caused by changes in the dimensionless cooling capacity Δ, defined by Eq. 3. Khinast et al. (1998) recently developed a numerical method to predict the boundaries of parameter regions in which a single-phase model of a cooled RFR has qualitatively different dynamic states (symmetric, asymmetric, and quasi-periodic motion).

A rational design, operation, and control of an RFR requires use of a mathematical model to predict the dynamic features of this forced periodic operation. A large variety of mathematical models may be used to simulate the behavior of a packed-bed reactor (Froment and Bischoff, 1990) from very simple to very detailed ones. State-of-the-art simulations of a fixed-bed reactor use a two-dimensional (2-D) model that accounts for axial and radial gradients. Use of this model in the dynamic simulation of an RFR requires repeated integration of a set of 2-D parabolic partial differential equations and an unreasonable computational effort. Thus, 1-D models are generally used to simulate the dynamics of the RFR. These include *pseudo-homogeneous* or *single-phase* models, which do not differentiate between the solid and fluid phase, and *heterogeneous* or *two-phase models*, which account separately for the species and energy balances in the solid and fluid phase. Single-phase models were used by several researchers, such as by Eigenberger and Nieken (1988), Matros (1989), Haynes et al. (1995), Nieken et al. (1995), Seiler and Emig (1997), Khinast and Luss (1997), and Khinast et al. (1998). 1-D two-phase models were used among others by van de Beld (1995) and Kulkarni and Dudukovic (1996, 1997). Even simpler models that describe the RFR in the limit of extremely short flow-reversal periods or of a traveling wave have been proposed and used (Matros, 1989; Nieken et al., 1995) but are not discussed here.

It is well established that inter- and intra-particle transport resistance may lead to steady-state multiplicity of catalyst pellets. In such cases, the rate expression in the single-phase model must include an effectiveness factor, which accounts for the transport resistances and the potential multiplicity. *A-priori* predictions of these effectiveness factors are simple for a first-order reaction in an adiabatic packed-bed reactor (Luss, 1976; Chang and Calo, 1980), but require iterative calculations in the other cases (Wedel and Luss, 1984).

The temperature profiles in RFRs are affected by the magnitude of the effective axial thermal dispersion. Vortmayer and Schaeffer (1974) suggested that if the effective axial heat conductivity of the single-phase model is chosen as

$$\lambda_{ax} = (1-\epsilon)\lambda_s + \lambda_g + \frac{u^2(\rho c_p)^2}{h a_v} \qquad (1)$$

the predictions of the two and single-phase models will be very similar. The third term in Eq. 1 accounts for the thermal dispersion caused by the heat-transfer resistance between the two phases. The above relation was derived under the assumption that the temperature front moves at a constant velocity of

$$w = \frac{u(\rho c_p)_g}{\epsilon(\rho c_p)_g + (1-\epsilon)(\rho c_p)_s}. \qquad (2)$$

This expression for the front velocity is valid for a bed in which no chemical reaction occurs. The velocity in a packed-bed reactor may deviate from this value. For zero heat conduction in the gas-phase, Vortmayer and Schaeffer (1974) derived another similarity relation, which is only based on the assumption of identical second-order derivatives of the gas and solid-phase temperatures. Chen and Luss (1989) derived a similar relation for the effective axial dispersion. Their derivation ignores the heat conductivity of the solid-phase λ_s, but accounts for changes in the front velocity from the prediction by Eq. 2. Previous studies of packed-bed reactors

Table 1. Parameters Used in the Simulations

a_v	1,426.0 m^2_{Surf}/m^3_{React}	u	1 m/s
D	$3 \cdot 10^{-5}$ m^2/s	ϵ	0.38
E/R	8,328.6 K	ΔT_{ad}	50 K
h	0.02 $kW/m^2 \cdot K$	λ_s	0.0 $kW/m \cdot K$
k_∞	$9.85 \cdot 10^6$ 1/s	λ_g	0.00026 $kW/m \cdot K$
k_c	0.115 m/s	$(\rho c_p)_g$	0.6244 $kJ/m^3 \cdot K$
L	4 m	$(\rho c_p)_s$	1382.0 $kJ/m^3 \cdot K$
$T_0 = T_{in}$	323 K		

(Chen and Luss, 1989) suggest that the predictions of the single- and two-phase model are rather similar when using the effective heat dispersion predicted by Eq. 1 even in cases where a wrong-way behavior occurs (transient temperature increase upon a reduction of the feed temperature). However, the predictions are quite different if the temperature front moves upstream. This uncommon behavior is usually not encountered in reverse-flow operation in which the temperature front and the fluid move in the same direction.

The main objective of this study is to determine if and under what conditions there is a difference in the quantitative and qualitative predictions of the RFR dynamics by the single and two-phase models when catalyst pellet multiplicity does not occur at any point in the reactor. Previous studies revealed chaotic behavior of an RFR described by the two-phase model (Rehacek et al., 1992, 1998). One of our objectives is to check if this chaotic behavior can be predicted also by the single-phase model.

Numerical Procedure

The single- and two-phase model of the RFR are well established and described in the Appendix. The values of the parameters used in the simulations are reported in Table 1. The flow reversal period t_f and the cooling capacity Δ, defined as

$$\Delta = \frac{a_W U_W L}{u(\rho c_p)_g}, \tag{3}$$

are used as the bifurcation parameters in this study.

Previous simulations by Rehacek et al. (1992, 1998) and Khinast et al. (1998) showed that cooling of an RFR can lead to surprising stability and dynamic features. In general the stability of periodic solutions is determined by studying the spectrum, that is, the eigenvalues, of the *monodromy matrix* M. The monodromy matrix describes the evolution of a small perturbation over one period. A periodic solution is stable when the absolute values of all the (possibly complex) eigenvalues of M are smaller than unity. When a single eigenvalue λ of the monodromy matrix crosses the unit circle in the complex plane, the periodic solution becomes unstable. At a *limit* point, such as an extinction or ignition point, one eigenvalue crosses the unit circle at $+1$. The symmetric states loose stability and become asymmetric when the largest eigenvalue crosses the unit circle at -1 (Khinast et al., 1998). Quasi-periodic states are obtained when a pair of complex conjugate eigenvalues crosses the unit circle. Period-q states emerge when a complex pair of eigenvalues crosses the unit circle exactly at the angle $\varphi = 2\pi p/q$, where p and q are integers. Phase-locking makes the existence of period-q solutions in the neighborhood of this exact bifurcation locus possible outside of the unit circle. Note, that for a large q, that motion is very difficult to distinguish from a quasi-periodic one. The monodromy matrices for both the single- and two-phase models were computed by integration of the sensitivity equations (see Khinast et al., 1998) and the eigenvalues were computed by the algorithm RG in EISPACK.

We determine the periodic states of the RFR by the direct computation approach first proposed by Gupta and Bhatia (1991) for the RFR. In this method a set of initial temperature and concentrations profiles is found by an iterative method such that these initial profiles are mirror images of those at the end of a flow-reversal period, that is, by enforcing

$$y(t = 0, x) = y(t = t_f, 1 - x), \tag{4}$$

where y denotes the spatial temperature and concentrations profiles. A Newton or quasi-Newton method is used to find an initial profile $y(t = 0, x)$ that satisfies Eq. 4 after integration of the model equations over one flow-reversal period $y(t = t_f)$, that is, a *shooting method* in time is implemented. Clearly, only symmetric states satisfy Eq. 4. Asymmetric states may be found by integration over two flow-reversal periods, and period-n solutions by integration over $2n$ flow-reversal periods. In contrast to dynamic simulation, which requires the simulation of many flow reversals in order to converge to the final quasi-stationary states, the direct method enables a very fast and efficient determination of these periodic states. Another advantage of this method is that it allows for a direct application of singularity and Floquet theory to the RFR. Thus, the boundaries between parameter regions with qualitatively different bifurcation diagrams (Khinast and Luss, 1997) or different dynamic features (Khinast et al., 1998) may be determined efficiently.

In our simulations we used the method of finite differences to discretize the spatial derivatives and the DA-solver LIMEX (Deuflhard et al., 1987) to integrate the resulting set of ordinary differential equations. Use of Broyden's method in combination with continuation techniques and a global update strategy enabled a very efficient numerical determination of the bifurcation diagrams (describing the dependence of the reactor states on an operating condition) and maps of regions with qualitatively different types of bifurcation diagrams or dynamic features. Details of the numerical method were presented by Khinast and Luss (1997) and Khinast et al (1998).

Dynamic Features of the Two Models

Extensive simulations were carried out to determine and compare the dynamic features of the single- and two-phase models. We used the axial thermal dispersion predicted by Eq. 1 in all the simulations. We examined mainly the impact of the cooling capacity Δ and the flow reversal period t_f. The model parameters were chosen so that no particle steady-state multiplicity can occur at any point in the reactor.

First, we constructed the loci of the limit points and of the symmetry loss points of the single-phase model in the (Δ, t_f) plane (Figure 3) using the method described by Khinast et al. (1998). The corresponding loci of the two-phase model are

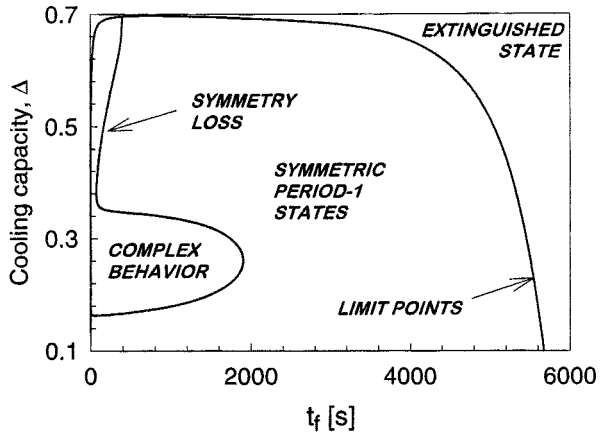

Figure 3. Map of regions with qualitatively different dynamic behavior of an RFR.

Boundaries are shown in the Δ-t_f plane.

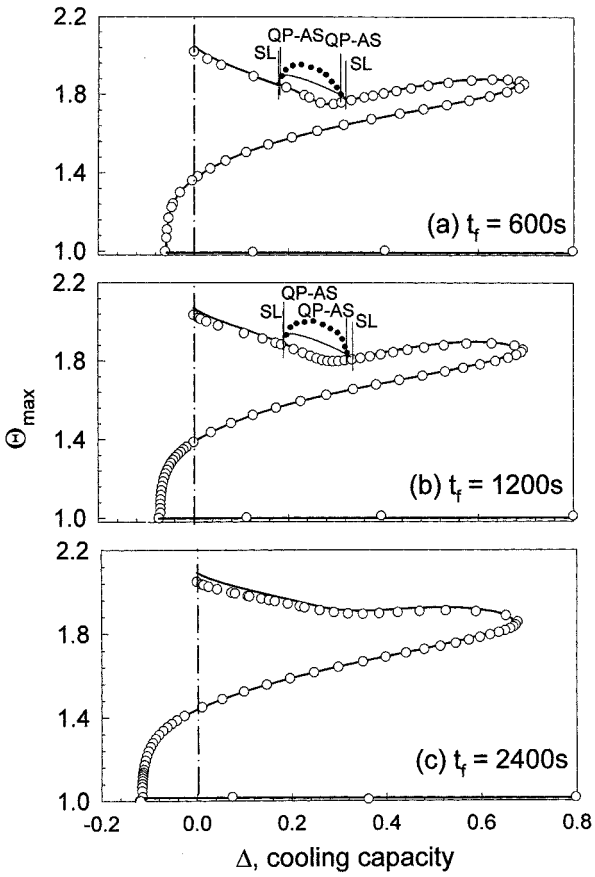

Figure 4. Dependence of the maximum dimensionless temperature on the cooling capacity Δ for three different flow reversal periods t_f.

Thick solid lines = single-phase mode; ○ = two-phase model; thin solid lines = asymmetric states; ●●● = quasi-periodic states.

very close to those of the single-phase model and the difference between the two cannot be clearly shown on this graph. The cooled RFR has a nonextinguished state in the region bounded by the limit point locus. Clearly, only extinguished states exist outside this boundary for a high cooling capacity (reaction cannot be sustained) or flow-reversal period (temperature front exits the reactor). The RFR attains nonsymmetric and complex dynamic behavior in the region bounded by the symmetry-loss locus. We conducted extensive simulations in this parameter region, as the behavior in this region is more sensitive to the parameter values.

In order to focus on interesting parameter values we constructed the bifurcation diagrams of the symmetric states for both models (Figure 4) and determined the bifurcation points at which these become asymmetric (symmetry loss bifurcation points, denoted as SL) and quasi-periodic (quasi-periodic asymmetric bifurcation points, denoted as QP-AS). The bifurcation diagrams describe the dependence of the maximum RFR temperature Θ_{max} of the symmetric states on the cooling capacity Δ for three different flow-reversal periods t_f. In addition the figure shows the branches of the asymmetric and quasi-periodic states, which exist for $t_f = 600$ s and 1,200 s. Such states do not exist for $t_f = 2{,}400$ s. These branches are shown only for the single-phase model as the branches of the two-phase model are very close and the difference cannot be shown on this graph. Desirable, stable high-conversion states exist only on the high-temperature branch. These high-conversion states exist for all cooling capacities smaller than that of the extinction point at $\Delta \approx 0.7$. For higher cooling capacities, only an extinguished state exists. A stable extinguished state ($\Theta_{max} \approx 1.02$) exists for all cooling capacities. The states on the intermediate branch are always unstable. The extinguished and intermediate branches emanate from a limit point for which the cooling capacity is negative. Clearly, states with negative cooling capacity have no physical meaning and are of no practical interest.

In general, the bifurcation diagrams of the periodic states of the single-phase (solid lines in Figure 4) and the two-phase model (open circles) are very similar, even at high cooling capacities. The agreement seems to be better for the shorter flow reversal periods. The main difference between the two models is the slightly higher Δ value of the extinction point of the two-phase model. Moreover, at low cooling capacities the two-phase model predicts maximum temperatures, which are slightly lower than those predicted by the single-phase model.

For all flow reversal periods, the highest bed temperature Θ_{max} is always obtained under adiabatic operation. Surprisingly, the bifurcation diagrams of Θ_{max} vs. Δ exhibit a local minimum at intermediate cooling capacities ($\Delta \approx 0.3$). This counterintuitive behavior is caused by a shift of the temperature profile from one with two maxima to one with a narrow single peak, illustrated in Figure 5 and described in more detail by Khinast et al. (1998).

Figure 6 describes the value of the largest eigenvalue λ_{max} of the Monodromy matrix (of the symmetric states) vs. Δ for $t_f = 600$ s, 1,200 s, and 2,400 s. Due to the sensitive dependence of the eigenvalues on the value of the parameters and the model type, they provide a good basis for a comparison of the model predictions. The eigenvalues for the single-phase model are represented by a solid line and those for the two-phase model by open circles. The symmetric states of the adiabatic RFR ($\Delta = 0$) are always stable, that is, the largest eigenvalue is real and smaller than unity. For both $t_f = 600$ s and 1,200 s (Figures 6a and 6b) and small Δ, the largest

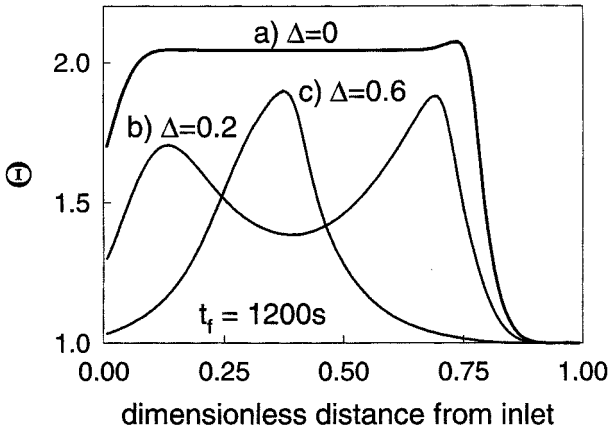

Figure 5. Dimensionless temperature profiles in the catalytic bed for (a) adiabatic operation, (b) small Δ, and (c) large Δ-values.

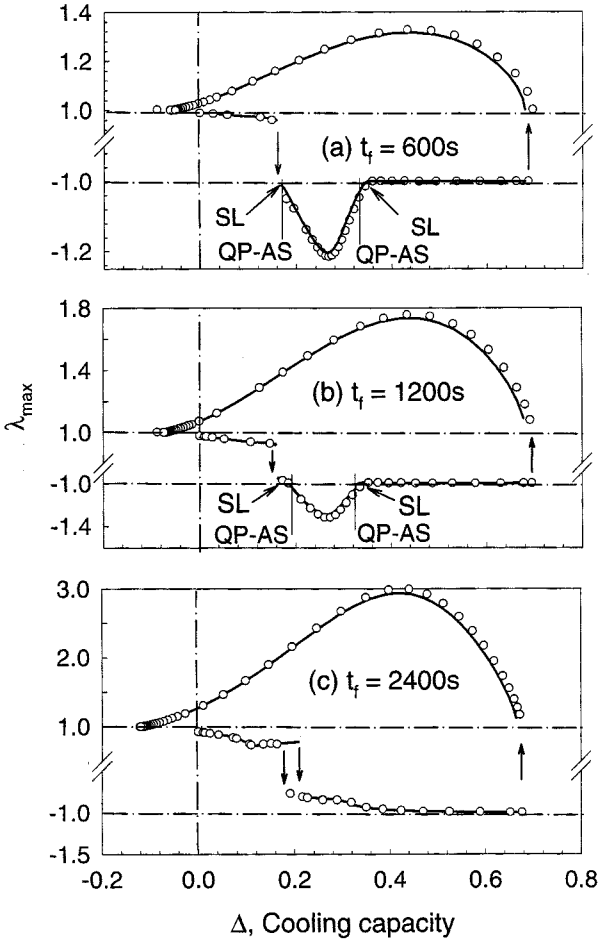

Figure 6. Dependence of the eigenvalue with maximum value on the cooling capacity Δ for three different flow-reversal periods t_f.

Solid lines = single-phase model; ○ = two-phase model. SL and QP-AS are the symmetry loss and quasi-periodic asymmetric bifurcation points of the single-phase model.

eigenvalue of the monodromy matrix M is real and smaller than unity and the symmetric states are stable. However at a critical Δ-value, the largest eigenvalue becomes equal to -1, causing a symmetry loss (SL) bifurcation. The symmetric states become unstable and instead a stable asymmetric period-1 state exists. The temperature and concentration profiles at the beginning and end of a flow-reversal period of these new emerging states are no longer mirror images of each other (see Figure 2b). The emerging asymmetric states exist only for a narrow range of Δ values before loosing their stability. As Δ is slightly increased, the asymmetric states become unstable and a stable quasi-periodic state emerges. At this quasi-periodic bifurcation from asymmetric states (QP-AS bifurcation), a conjugate complex pair of eigenvalues crosses the unit circle. The quasi-periodic states vanish upon a further increase in Δ at a second QP-AS point and again asymmetric states appear. At even higher cooling capacities, the symmetric states become stable again at a SL bifurcation. The emerging stable, symmetric states exist for all higher Δ values until the cooling causes eventual extinction of that branch at Δ-values of about 0.7. At this limit point, a real eigenvalue of M crosses the unit circle at $+1$. The two SL and two QP-AS bifurcation points for the two models are rather close to each other. For the sake of clarity, we show in Figures 4 and 6 those bifurcations only for the single-phase model. Figure 6c shows that for a flow-reversal period of 2,400 s all the symmetric states on the high-temperature branch are stable, as $|\lambda_{max}|$ is always smaller than unity.

It is interesting to note that the largest eigenvalues of M for both models are almost identical. Consequently, it may be concluded that both models will predict a very similar dynamic behavior in parameter regions where both models have a stable symmetric period-1 state. In the following section we shall report only simulations in the parameter range in which the two models have complex dynamic features, that is, the region bounded by the SL loci. In Figure 7 this region in the parameter space is shown, and it can be seen that the location of the predicted symmetry loss differs slightly for the two models. We mark on that figure the set of (Δ, t_f) values corresponding to the examples shown in Figures 8 and 9.

Figure 8 illustrates the temporal reactor center temperature for three cases for which $t_f = 600$ s. The cooling capacities of the three cases are within the quasi-periodic region for both models (see Figure 7), and none is close to a QP-AS bifurcation point. The figure shows that the temporal temperatures at the reactor center predicted by both models are very similar and quasi-periodic. The thickness of the band describes the change in the center temperature during one flow reversal period. In the case shown in Figure 8a and 8b ($\Delta = 0.2$) in addition to the forcing period of $\tau = 1$, a second period of approximately 135 flow reversals exists. In Figure 8c and 8d ($\Delta = 0.25$) the second period is about 80 flow reversals, while in Figures 8e and 8f ($\Delta = 0.3$), the motion is rather complex and the second period is approximately 200 flow reversals. The amplitude of the oscillations decreases as the cooling capacity gets close to the SL bifurcation points. However, the quasi-periodic motion becomes more complicated as Δ gets close to the QP-AS bifurcation point (at $\Delta =$ 0.327 for the single-phase model). The simulations show that, in general, the dynamic motions predicted by the two models

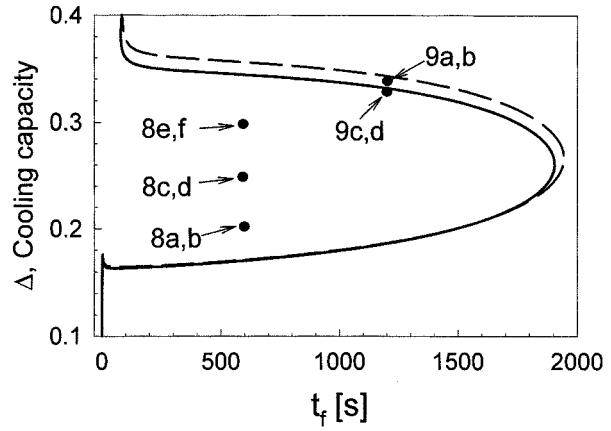

Figure 7. Symmetry loss loci in the Δ-t_f plane for the single and two-phase models.

Solid line = single-phase model; dashed line = two phase model.

are very similar over a wide range of operating conditions even in the quasi-periodic region.

Slight differences in the location of the SL and QP-AS bifurcation points of the two models cause differences in the dynamic features next to these bifurcations. This point is illustrated by the dynamic simulations shown in Figure 9 for $t_f = 1{,}200$ s. Figures 9a and 9b show the temporal center temperature for a case in which the cooling capacity is above the

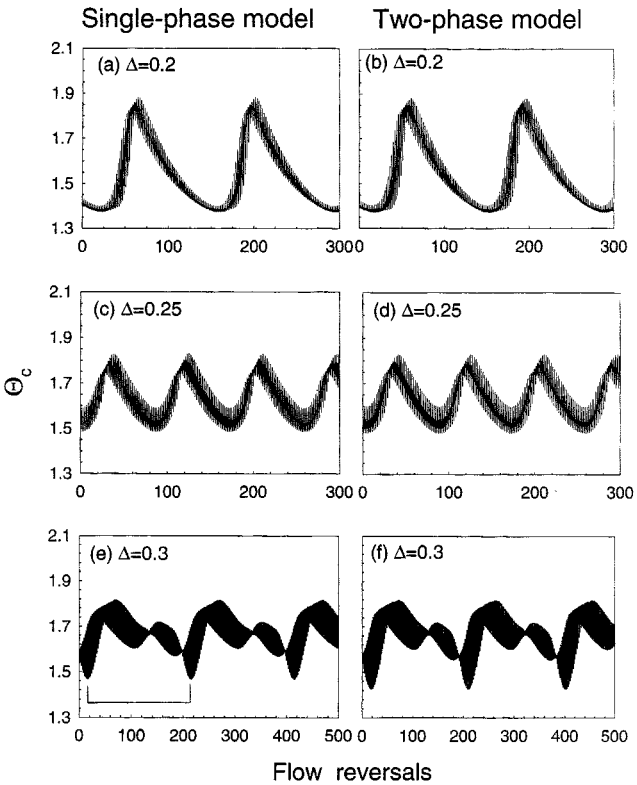

Figure 8. Temporal dependence of the reactor center dimensionless temperature on cooling capacity Δ for the two models at $t_f = 600$ s.

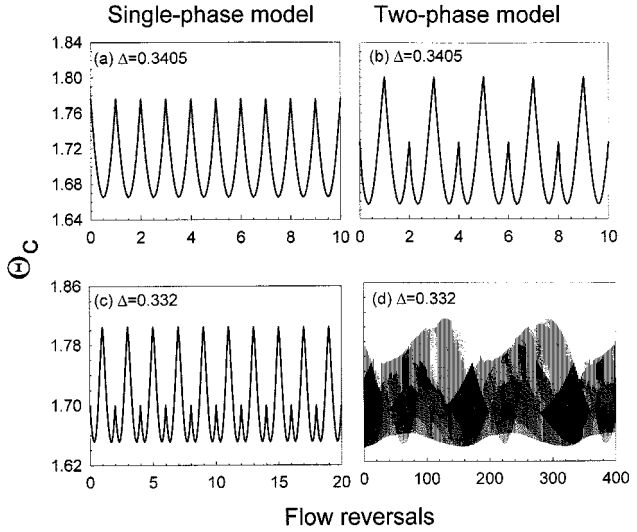

Figure 9. Temporal dependence of the reactor center dimensionless temperature on cooling capacity Δ for the two models at $t_f = 1{,}200$ s.

SL bifurcation point for the single-phase model, but below that of the two-phase model (see Figure 7). Thus, the single-phase model predicts a stable, symmetric state (Figure 9a), while the two-phase model predicts that an asymmetric state is stable (Figure 9b). Figure 9c and 9d describe a state in which $\Delta = 0.332$ is below the SL point of both models, but above the QP-AS of the single-phase model ($= 0.325$) and below that of the two phase model ($= 0.334$). Here, the single-phase model (Figure 9c) predicts asymmetric behavior, whereas the two-phase model predicts a complex quasi-periodic motion (Figure 9d).

Our simulations revealed that, within the region bounded by the two QP-AS loci, there exist small sections with rather complex quasi-periodic, as well as chaotic behavior. For a given flow-reversal period, these regions exist for slightly different sets of cooling parameters for the two models. Since the corresponding dynamic behavior is very sensitive to the parameter values in this complex region, even the qualitative dynamic features of the two models may be different for the same set of parameters. This behavior will be illustrated for a specific case for which $t_f = 1{,}200$ s. Here chaotic behavior was found in a Δ-range of (0.2995, 0.301) and (0.3097, 0.3112) for the single- and two-phase models, respectively.

To illustrate the development of chaos for the single-phase model, we consider first the simple quasi-periodic behavior shown in Figure 10. We constructed a corresponding Poincaré map by plotting of $\Delta\Theta_{av}(n)$ vs. $\Theta_{av}(n)$, where we define

$$\Theta_{av}(n) = \frac{1}{L}\int_0^L \Theta(nt_f, x)\,dx, \qquad n = 1,2,3,\ldots, \quad (5)$$

$$\Delta\Theta_{av}(n) = \frac{2}{L}\left[\int_0^{L/2}\Theta(nt_f, x)\,dx - \int_{L/2}^{L}\Theta(nt_f, x)\,dx.\right], \qquad n = 1,2,3,\ldots \quad (6)$$

$\Theta_{av}(n)$ is the average reactor temperature after the nth flow

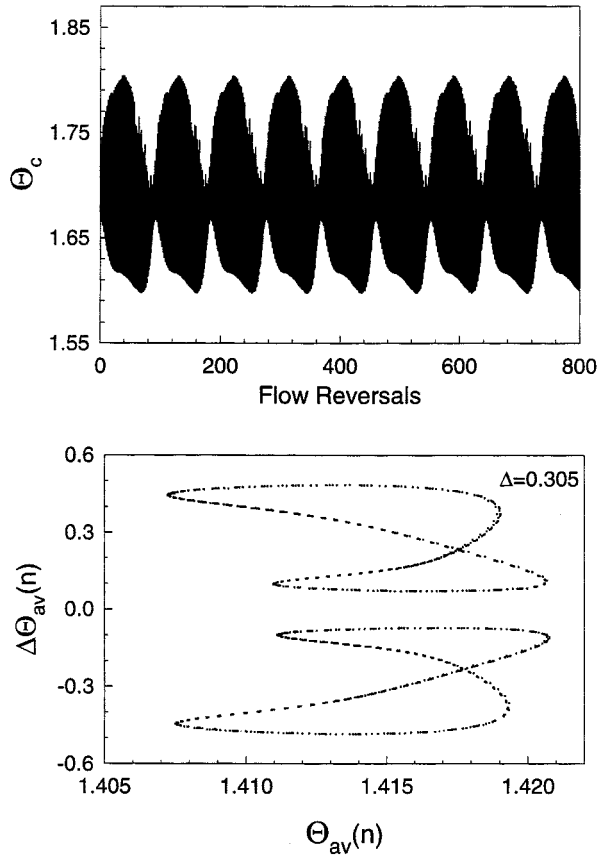

Figure 10. Temporal reactor center dimensionless temperature and corresponding Poincaré map for t_f = 1,200 s and Δ = 0.305 for the single-phase model.

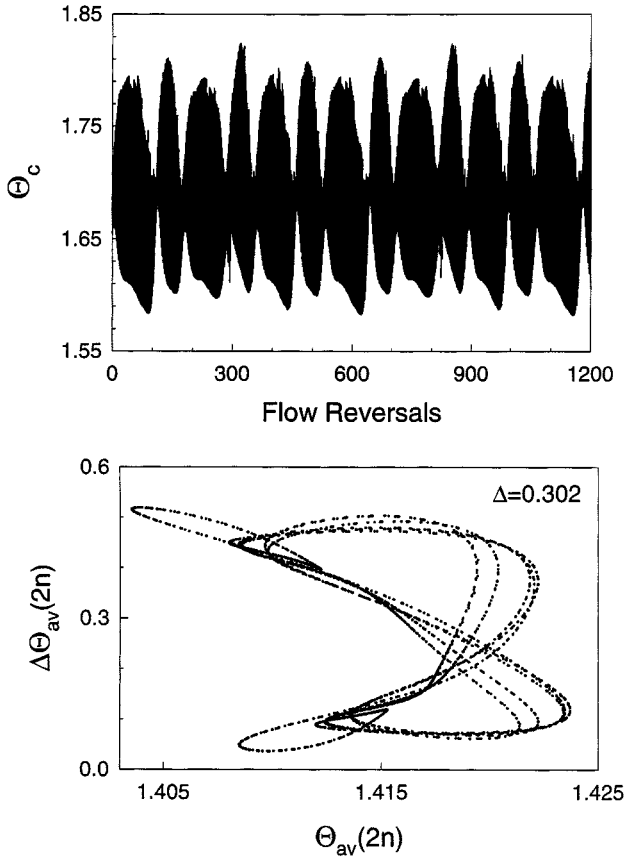

Figure 11. Complex quasi-periodic reactor center dimensionless temperature and corresponding Poincaré map at t_f = 1,200 s and Δ = 0.302 for the single-phase model.

reversal and $\Delta\Theta_{av}(n)$ is the corresponding averaged difference between the temperatures in the right and left half of the reactor. Clearly, the sign of $\Delta\Theta_{av}$ changes upon alternating flow reversal. For symmetric period-1 states, the Poincaré map consists of two points, both for the same $\Theta_{av}(n)$ value. For asymmetric period-1 states, the Poincaré map has two points, but not for the same $\Theta_{av}(n)$ values. The Poincaré map in Figure 10 consists of a set of points forming two closed curves, thus indicating quasi-periodic behavior. Each curve corresponds to one flow direction. Due to the similar information contained by the upper and lower part of the map, we show in other examples only the upper part of the map, which is equivalent to constructing a Poincaré map of $\Delta\Theta_{av}(2n)$ vs. $\Theta_{av}(2n)$, where n is an integer.

A 1% decrease of the cooling capacity from that in Figure 10 to 0.302 shifts the dynamics to the complex motion, described in Figure 11. The period of oscillations in this case ($\sim$ 520 flow reversals) is about six times that in Figure 10 ($\sim$ 88 flow reversals) and the time series includes six different peaks. The Poincaré map consists of six loops indicating a complex quasi-periodic motion, which may be due to a *period-multiplying bifurcation* of the quasi-periodic motion. Decreasing further the cooling capacity leads to chaotic motion. Figure 12 shows the temporal variation of the average reactor temperature and the corresponding Poincaré map of a chaotic attractor for $\Delta = 0.2996$. This finding is the first report of chaotic dynamics of an RFR described by a single-phase model.

The chaotic motion of the two-phase model exists for slightly higher Δ values than that for the single-phase model. Figure 13 shows that for $\Delta = 0.3$, the two-phase model exhibits simple quasi-periodic motion. (The single-phase model predicts a chaotic motion for this Δ-value.) It also shows that the quasi-periodic motion becomes more intricate as Δ is increased. The period of the motion for $\Delta = 0.302$ and 0.305 is four times and twice that for $\Delta = 0.3$. The complex motion shown in Figure 13 for the two-phase model at $\Delta = 0.305$ is rather different from that of single-phase model at the same set of parameters (Figure 10). Similarly, the quasi-periodic motion shown in Figure 13 for the two-phase model at $\Delta = 0.302$ is rather different from that in Figure 11 for the single-phase model and the same set of parameters.

The two-phase model becomes chaotic at $\Delta = 0.3097$. Figure 14 shows a chaotic state obtained at $\Delta = 0.31$. For the same set of parameters, the single-phase model predicts a simple quasi-periodic motion similar to that shown in Figure 10. However, the Poincaré map of the chaotic state for the two-phase model (Figure 14) is rather similar to that obtained for the single-phase model (Figure 12) for a slightly different set of parameters.

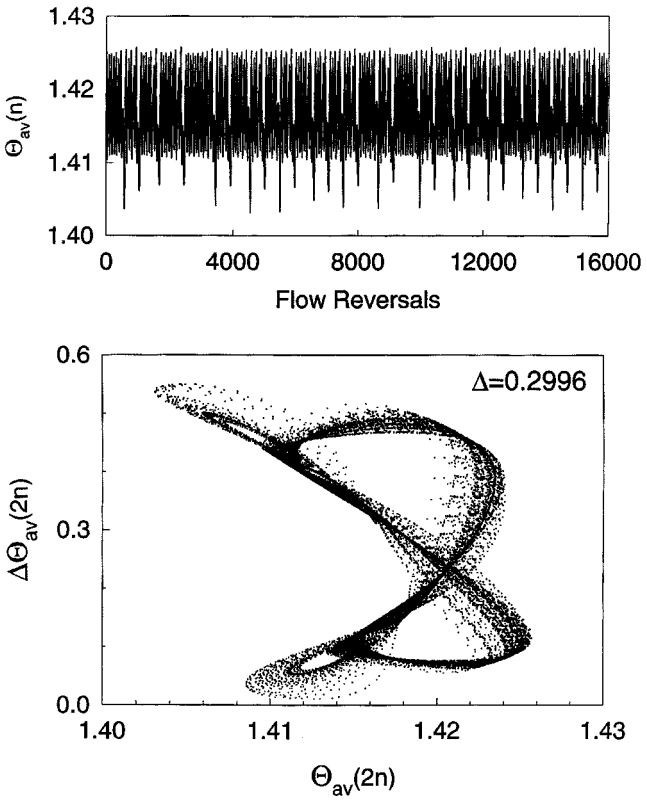

Figure 12. Chaotic temporal reactor center dimensionless temperature and corresponding Poincaré map at t_f = 1,200 s and Δ = 0.2996 for the single-phase model.

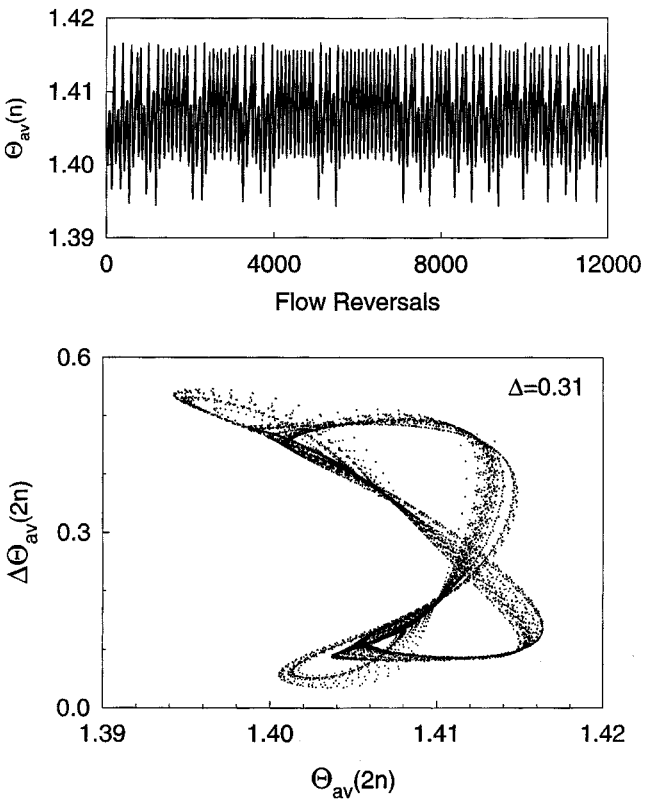

Figure 14. Chaotic reactor center dimensionless temperature and Poincaré map at t_f = 1,200 s and Δ = 0.31 for the two-phase model.

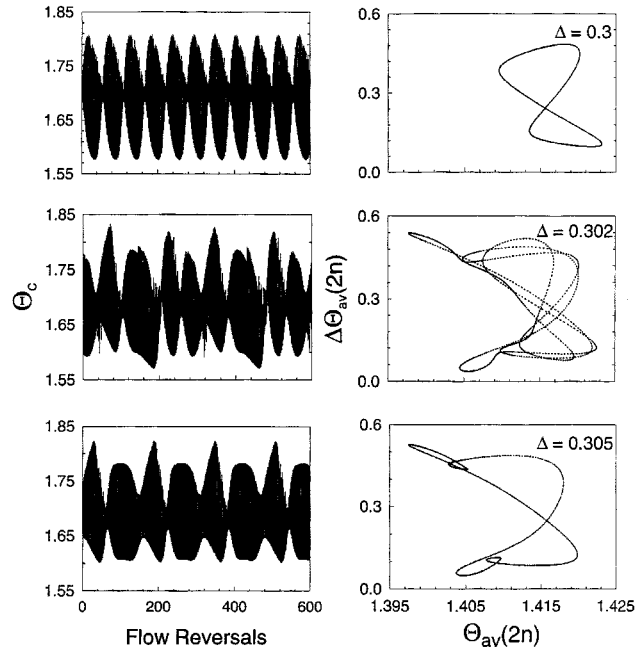

Figure 13. Quasi-periodic reactor center dimensionless temperature and corresponding Poincaré map at t_f = 1,200 s and three different cooling capacities for the two-phase model.

In our simulations the coolant and feed temperature were the same. Rehacek et al. (1992, 1998) found that a two-phase model of the RFR exhibits chaotic features when the feed temperature (= 730 K) was much higher than the coolant temperature (310 K). Figure 15 shows the computed center bed temperature for the two- and single-phase model for the parameter values used by Rehacek et al. (1992, 1998). Our simulations show that while the two-phase model exhibits chaotic features, the single-phase model predicts a much simpler period-1 asymmetric motion. We were not successful in our attempt to find a region with chaotic behavior of the single-phase model for parameters close to those used by Rehacek et al. (1992, 1998). A series of simulations (Figure 16) was conducted to check the impact of the large temperature difference on the dynamics of the two-phase model. When the feed temperature was decreased (left column of Figure 16), the behavior became more regular. The behavior was quasi-periodic for T_f = 690 K, period-1 asymmetric for T_f = 670 K, and period-1 symmetric for T_f = 630 K. Simulations of the single-phase model for the same set of parameters led to a symmetric period-1 behavior in the three cases, indicating a significant qualitative difference in the predictions of the two models.

The above simulations suggested that the large temperature difference between the two phases in part of the bed, due to the temperature difference between the feed and coolant (see Figure 17), is the cause for the qualitative difference in the predictions of the two models. To check this con-

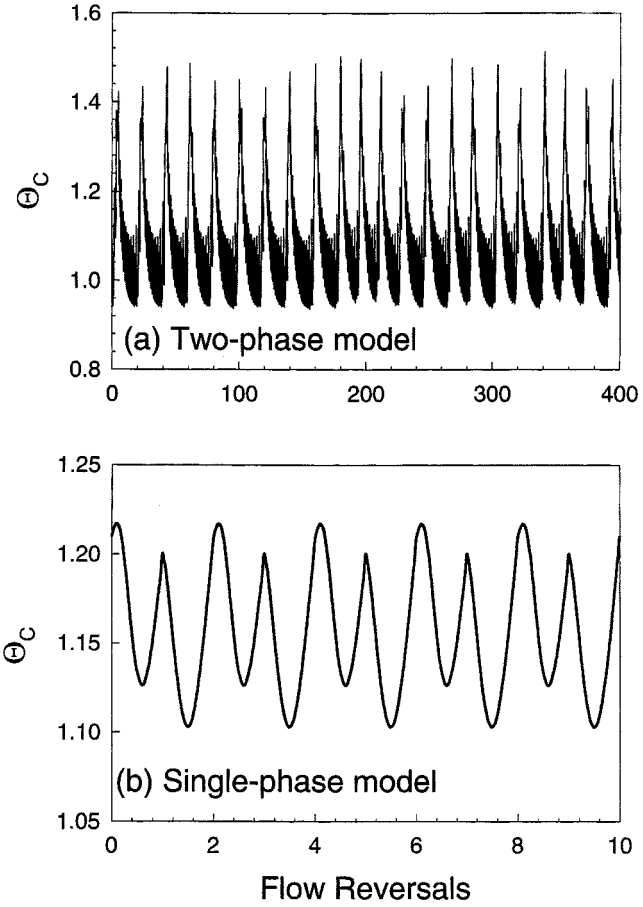

Figure 15. Temporal reactor center dimensionless temperature for the set of parameters used by Rehacek et al. (1998).

$Pe_h^* = 144{,}000$; $T_R = 470$. (a) Two-phase model; (b) single-phase model.

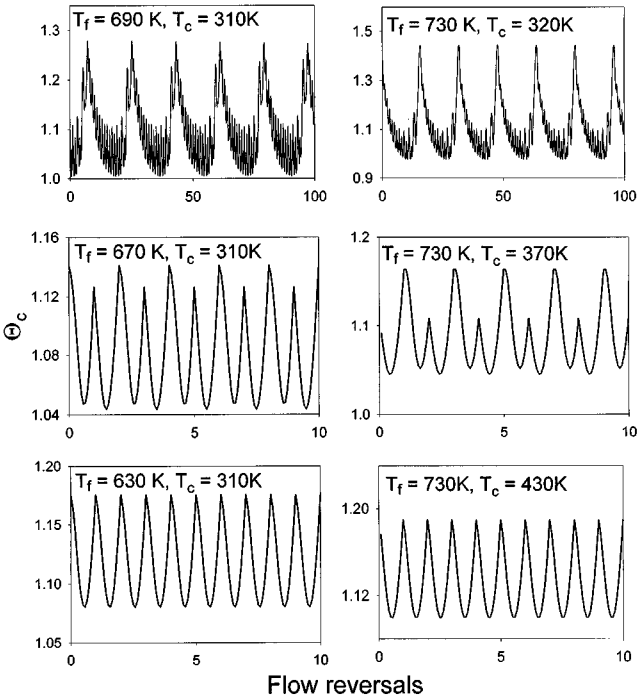

Figure 16. Reactor center dimensionless temperature for the set of parameters used by Rehacek et al. (1998) for different feed (T_f) and coolant (T_c) temperatures.

Remaining parameters are identical to those in Figure 15.

jecture, simulations were carried out for the two-phase model for the same feed temperature and increasing values of the coolant temperatures (right column of Figure 16). Again, decreasing the temperature difference between the two phases led to a simpler dynamic behavior of the two-phase model. The state was quasi-periodic for $T_c = 320$ K, period-1 asymmetric for $T_c = 370$ K, and period-1 symmetric for $T_c = 430$ K. Simulations of the single-phase model revealed an asymmetric period-1 solution for $T_c = 320$ K and period-1 symmetric in the other two cases. These and other simulations showed that the two models may predict different dynamic features of the cooled RFR when large temperature differences exist between the feed and coolant.

Summary and Conclusions

The simulations indicate that in most, but not all, cases the single- and two-phase models predict similar dynamic behavior of an RFR when using the effective dispersion coefficient suggested by Vortmayer and Schaeffer (1974). For an adiabatic RFR, both models usually predict a very similar symmetric period-1 state. The cooled RFR may exhibit much more intricate dynamic features, especially for intermediate levels of cooling when the flow-reversal period is much shorter than that needed for the temperature wave to transverse the reactor. As shown by Rehacek et al. (1992, 1998), Salinger and Eigenberger (1996b), and Khinast et al. (1998), the cooled reactor may attain asymmetric states as well as quasi-periodic or even chaotic states. The simulations show that, even for a cooled RFR, the dynamic behaviors predicted by the two models are usually very similar, even when they are complex (Figure 8). However, the similarity of the predictions may

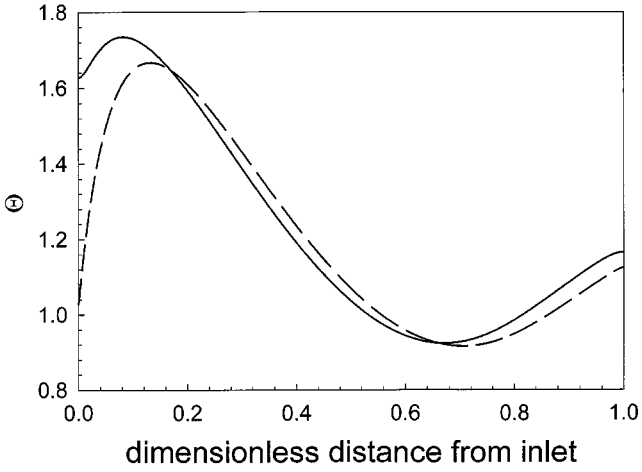

Figure 17. Gas (– – –) and solid-phase (——) dimensionless temperature profiles just after a flow reversal for the set of parameters used by Rehacek et al. (1998).

break down when the parameters are close to one of the dynamic bifurcation loci. Figures 12–14 illustrate such a case in which the two models predict chaotic behavior for slightly different parameter values. Clearly, when the dynamic bifurcations occur for different parameters, the two models predict qualitatively different dynamics for parameters between these two bifurcations (such as Figure 9).

The chaotic attractor exhibited by the two models (Figures 12 and 14) seems to have a relatively simple structure and low dimension. Some of the quasi-periodic states near that region, such as that shown in Figures 11 and 13 are rather unusual. Of particular interest is the period-doubling of the quasi-periodic motion in Figure 13. It would be of interest to gain a physical understanding of these complex dynamics and an ability to predict the operating conditions under which these occur. While in practice one would try to avoid operation under conditions leading to complex dynamics, their features are of academic interest.

The predicted heat loss and reaction rate of the single-phase model are based on the average cross-section temperature, which is very close to that of the solid. The heat loss of the two-phase model is based on the fluid temperature and the reaction rate on the solid temperature. In the common case that the solid-fluid temperature difference is small, the predictions of the two models are very close. However, that similarity in the predictions breaks down when a large temperature difference exists between the two phases in a section of the reactor (Figures 15–16). Note that, for cases of strong cooling, the effective dispersion relation of Vortmayer and Schaeffer (1974), which was derived for an adiabatic reactor, should be modified, and one may have to use different wall heat-transfer coefficients in the two models. Large solid-fluid temperature differences are encountered also when particle steady-state multiplicity occurs, a behavior not encountered in any of our simulations. The safest simulation of cases involving large solid-fluid temperature differences is probably via a two-phase, 2-D model.

Acknowledgments

We gratefully acknowledge the financial support by the ACS-PRF and Mobil Foundation. We are thankful to the Dept. of Chemical Engineering, AMVT, Graz University of Technology in Austria, for using their computer facilities.

Notation

a_V = specific particle surface area, m^2_{Surf}/m^3_{React}
a_W = specific reactor wall surface, m^2_{wall}/m^3_{React}
c = gas-phase concentration, $kmol/m^3$
c^* = concentration at the particle surface, $kmol/m^3$
D = gas diffusion coefficient, m^2/s
E = activation energy, kJ/kmol
h = heat-transfer coefficient, $kW/(m^2_p K)$
$-\Delta H$ = heat of reaction, kJ/kmol
k_c = mass-transfer coefficient, m/s
k_∞ = frequency factor, 1/s
L = reactor length
R = universal gas constant, kJ/kmol/K
t = time, s
T = gas-phase temperature, K
T^* = solid-phase temperature, K
u = superficial gas velocity, m/s
U_w = heat-transfer coefficient at reactor wall, $kW/(m^2_R \cdot K)$
w = velocity of the thermal wave, m/s
x = axial coordinate, m

Greek letters

ϵ = void fraction
η = effectiveness factor
λ = thermal conductivity, kW/m/K
Θ = dimensionless temperature, $\Theta = T/T_0$
ρc_p = volumetric heat capacity, $kJ/m^3/K$
τ = dimensionless time, $\tau = t/t_f$

Indices

ax = axial
c = flow reversal coolant, center
g = gas
0 = feed
s = solid
w = wall

Literature Cited

Blanks, R. F., T. S. Wittrig, and D. A. Peterson, "Bidirectional Adiabatic Synthesis Gas Reactor," *Chem. Eng. Sci.*, **45**, 2407 (1990).

Bobrova, L. N., E. M. Slavinskaya, A. S. Noskov, and Y. S. Matros, "Unsteady-State Performance of NO_x Catalytic Reduction by NH_3," *React. Kinet. Catal. Lett.*, **37**, 267 (1988).

Boreskov, G. K., Yu. Sh. Matros, and O. V. Kiselev, "Catalytic Processes Carried Out Under Nonstationary Conditions: Thermal Front in a Fixed Bed of Catalysts," *Kinet. Catal.*, **20**, 773 (1979).

Boreskov, G. K., and Yu. Sh. Matros, "Unsteady-State Performance of Heterogeneous Catalytic Reactions," *Catal. Rev.-Sci. Eng.*, **25**, 551 (1983).

Chang, H. C., and J. M. Calo, "Exact Universal Uniqueness Criteria for the Adiabatic Tubular Packed Bed Reactor," *Chem. Eng. Sci.*, **35**, 1611 (1980).

Chen, Y. C., and D. Luss, "Wrong-Way Behavior of Packed-Bed Reactors: Influence of Interphase Transport," *AIChE J.*, **35**, 1148 (1989).

Cottrell, F. G., "Purifying Gases and Apparatus Therefor," U.S. Patent No. 2,171,733 (June 21, 1938).

Deuflhard, P., E. Hairer, and J. Zugck, "One-Step and Extrapolation Methods for Differential-Algebraic Systems," *Numer. Math.*, **51**, 1 (1987).

Eigenberger, G., and U. Nieken, "Catalytic Combustion with Periodic Flow Reversal," *Chem. Eng. Sci.*, **43**, 2109 (1988).

Frank-Kamenetskii, D. A., *Diffusion and Heat Transfer in Chemical Kinetics*, Princeton Univ. Press, Princeton, NJ (1955).

Froment, G. F., and K. B. Bischoff, *Chemical Reactor Analysis and Design*, Wiley, New York (1990).

Gupta, V. K., and S. K. Bhatia, "Solution of Cyclic Profiles in Catalytic Reactor Operation with Periodic Flow Reversal," *Computers Chem. Eng.*, **15**, 229 (1991).

Haynes, T. N., C. Georgakis, and H. S. Caram, "The Design of Reverse Flow Reactors for Catalytic Combustion Systems," *Chem. Eng. Sci.*, **50**, 401 (1995).

Khinast, J., and D. Luss, "Mapping Regions with Different Bifurcation Diagrams of a Reverse Flow Reactor," *AIChE J.*, **43**, 2034 (1997).

Khinast, J., A. Gurumoorthy, and D. Luss, "Complex Dynamic Features of a Cooled Reverse-Flow Reactor," *AIChE J.*, **44**, 1128 (1998).

Kulkarni, M. S., and M. P. Dudukovic, "A Bidirectional Fixed-Bed Reactor for Coupling of Exothermic and Endothermic Reactions," *AIChE J.*, **42**, 2897 (1996).

Kulkarni, M. S., and M. P. Dudukovic, "Periodic Operation of Asymmetric Bidirectional Fixed-Bed Reactors: Energy Efficiency," *Chem. Eng. Sci.*, **42**, 1777 (1997).

Luss, D., "Uniqueness and Multiplicity Criteria for Porous Catalytic Pellets and Packed-Bed Reactors within Uniform Intraparticle Temperature," *Proc. Int. Symp. Chem. React. Eng., Heidelberg*, **2**, 487, Dechema (1976).

Matros, Yu. Sh., *Catalytic Processes Under Unsteady State Conditions*, Elsevier, Amsterdam (1989).

Matros, Yu. Sh., and G. A. Bunimovich, "Reverse-Flow Operation in Fixed Bed Catalytic Reactors," *Cat. Rev. Sci. Eng.*, **38**, 1 (1996).

Neophytides, S. G., and G. G. Froment, "A Bench Scale Study of

Reversed Flow Methanol Synthesis,'' *Ind. Eng. Chem. Res.*, **31**, 1583 (1992).
Nieken, U., G. Kolios, and G. Eigenberger, ''Fixed-Bed Reactors with Periodic Flow Reversal: Experimental Results for Catalytic Combustion,'' *Cat. Today*, **20**, 355 (1994).
Nieken, U., G. Kolios, and G. Eigenberger, ''Limiting Cases and Approximate Solutions for Fixed-Bed Reactors with Periodic Flow Reversal,'' *AIChE J.*, **41**, 1915 (1995).
Rehacek, J., M. Kubicek, and M. Marek, ''Modeling of a Tubular Reactor with Flow Reversal,'' *Chem. Eng. Sci.*, **47**, 2897 (1992).
Rehacek, J., M. Kubicek, and M. Marek, ''Periodic, Quasiperiodic and Chaotic Spatiotemporal Patterns in a Tubular Catalytic Reactor with Periodic Flow Reversal,'' *Comput. Chem. Eng.*, **22**, 283 (1998).
Salinger, A. G., and G. Eigenberger, ''The Direct Calculation of Periodic States of the Reverse-Flow Reactor: 1. Methodology and Propane Combustion Results,'' *Chem. Eng. Sci.*, **51**, 4903 (1996a).
Salinger, A. G., and G. Eigenberger, ''The Direct Calculation of Periodic States of the Reverse Flow Reactor: 2. Multiplicity and Instability,'' *Chem. Eng. Sci.*, **51**, 4915 (1996b).
Seiler, H., and G. Emig, ''Reduction-Oxidation-Cycling in a Fixed Bed Reactor with Periodic Flow Reversal,'' *Symposium Proceedings, Dynamics and Reaction Kinetics in Heterogeneous Catalysis*, Antwerpen, Belgium (1997).
van de Beld, B., and K. R. Westerterp, ''Air Purification by Catalytic Oxidation in a Reactor with Periodic Flow Reversal,'' *Chem. Eng. Technol.*, **17**, 217 (1994).
van de Beld, B., ''Air Purification by Catalytic Oxidation in a Reverse Flow Reactor,'' PhD Thesis, University of Twente, Enschede, The Netherlands (1995).
Vortmeyer, D., and R. J. Schaefer, ''Equivalence of One- and Two-Phase Models for Heat Transfer Processes in Packed Beds: One Dimensional Theory,'' *Chem. Eng. Sci.*, **29**, 484 (1974).
Watson, E. W., ''Method and Apparatus for Reacting for Sulfur Dioxide and Natural Gas,'' U.S. Patent No. 3,865,927 (1975).
Wedel, S., and D. Luss, ''Steady-State Multiplicity Features of an Adiabatic Fixed-Bed Reactor with Langmuir-Hinshelwood Kinetics: CO or CO_2 Methanation,'' *IEC Fundls*, **23**, 280 (1984).
Züfle, H., and T. Turek, ''Catalytic Combustion in a Reactor with Periodic Flow Reversal: 1. Experimental Results,'' *Chem. Eng. Proc.*, **36**, 327 (1997).

Appendix

The 1-D, two-phase model accounts for axial heat and mass dispersion in the gas phase, for heat conduction in the solid phase, and for mass and heat transfer between the fluid and the catalyst. We assume that all the physical properties are independent of the temperature and concentration and that the pressure loss along the length of the catalytic bed is negligible. An additional assumption is that cooling occurs only via the gas phase due to the negligible contact area between the catalyst particles and the reactor wall. The energy balances for the gas and solid phase are:

$$\epsilon(\rho c_p)_g \frac{\partial T}{\partial t} = -u(\rho c_p)_g \frac{\partial T}{\partial x} + \epsilon\lambda_g \frac{\partial^2 T}{\partial x^2} + ha_V(T^* - T) - U_W a_W(T - T_c), \quad (7)$$

$$(1-\epsilon)(\rho c_p)_s \frac{\partial T^*}{\partial t} = (1-\epsilon)\lambda_s \frac{\partial^2 T^*}{\partial x^2} - ha_v(T^* - T) + (-\Delta H)\eta k_\infty \exp[-E/RT^*]c^* \quad (8)$$

where the * denotes the solid phase. The mass balances for the gas and solid phase are

$$\epsilon \frac{\partial c}{\partial t} = -u\frac{\partial c}{\partial x} + \epsilon D \frac{\partial^2 c}{\partial x^2} + k_c a_v(c^* - c) \quad (9)$$

$$(1-\epsilon)\frac{\partial c^*}{\partial t} = -k_c a_v(c^* - c) - \eta k_\infty \exp[-E/RT^*]c^* \quad (10)$$

In Eqs. 7–10 η is the particle effectiveness factor, which we assumed to be unity, and T_c is the coolant temperature. The boundary conditions for the flow in the right direction are

$$-\frac{\epsilon\lambda_g}{u(\rho c_p)_g}\frac{\partial T}{\partial x} = T_0 - T; \qquad -\frac{\epsilon D}{u}\frac{\partial c}{\partial x} = c_0 - c;$$

$$\frac{\partial T^*}{\partial x} = \frac{\partial c^*}{\partial x} = 0 \quad \text{at} \quad x = 0 \quad (11)$$

$$\frac{\partial T}{\partial x} = \frac{\partial c}{\partial x} = \frac{\partial T^*}{\partial x} = \frac{\partial c^*}{\partial x} = 0 \quad \text{at} \quad x = L, \quad (12)$$

where L is the length of the reactor. Symmetric boundary conditions apply for flow in the left direction.

Assuming that c^* is in a quasi-stationary state, it may be expressed as a function of the rate constant, the effectiveness-factor, and the mass-transfer coefficient. This leads to the following heat and mass balance of the single-phase model

$$(1-\epsilon)(\rho c_p)_s \frac{\partial T}{\partial t} = \lambda_{ax}\frac{\partial^2 T}{\partial x^2} - u(\rho c_p)_g \frac{\partial T}{\partial x} - U_W a_W(T - T_c) + (-\Delta H)\frac{\eta k_\infty k_c a_V \exp[-E/RT]}{k_c a_V + \eta k_\infty \exp[-E/RT]}c \quad (13)$$

$$\epsilon\frac{\partial c}{\partial t} = -u\frac{\partial c}{\partial x} + \epsilon D\frac{\partial^2 c}{\partial x^2} - \frac{\eta k_\infty k_c a_V \exp[-E/RT]}{k_c a_V + \eta k_\infty \exp[-E/RT]}c \quad (14)$$

The boundary conditions for flow to the right are

$$-\frac{\lambda_{ax}}{u(\rho c_p)_g}\frac{\partial T}{\partial x} = T_0 - T, \quad -\frac{\epsilon D}{u}\frac{\partial c}{\partial x} = c_0 - c \quad \text{at} \quad x = 0 \quad (15)$$

$$\frac{\partial T}{\partial x} = \frac{\partial c}{\partial x} \quad \text{at} \quad x = L \quad (16)$$

Manuscript received Aug. 28, 1998, and revision received Dec. 10, 1998.